

Sound Attenuation at Terahertz Frequencies and the Boson Peak of Vitreous Silica

G. Baldi,^{1,2,*} V. M. Giordano,¹ G. Monaco,¹ and B. Ruta¹

¹European Synchrotron Radiation Facility, BP220, 38043 Grenoble, France

²IPCF-CNR, UOS di Roma, 00185 Roma, Italy

(Received 15 December 2009; published 11 May 2010)

The propagation and damping of the acoustic excitations in vitreous silica is measured at terahertz frequencies using inelastic x-ray scattering. The apparent sound velocity shows a marked dispersion with frequency while the sound attenuation undergoes a crossover from a fourth to a second power law frequency dependence. This finding solves a recent controversy concerning the location of this crossover in vitreous silica, clarifying that it occurs at the position of the glass-characteristic excess of vibrational modes known as boson peak, and thus establishing a direct connection between boson peak and acoustic dispersion curves.

DOI: 10.1103/PhysRevLett.104.195501

PACS numbers: 63.50.Lm, 62.65.+k, 64.70.ph

The low temperature thermal properties of amorphous materials strongly differ from those of the corresponding crystalline structures. The specific heat, $C(T)$, of glasses is marked by an excess over the $\propto T^3$ Debye prediction, which appears at temperatures around 10 K as a maximum in $C(T)/T^3$ [1]. The maximum is associated to an excess of vibrational modes over the $\propto \nu^2$ Debye prediction at frequencies around 1 THz. This excess is best visible as a maximum, known as boson peak (BP), in the reduced vibrational density of states, $g(\nu)/\nu^2$ [2]. In the same temperature range where $C(T)/T^3$ has a maximum, the thermal conductivity presents a characteristic plateau, whose origin has been strongly debated in the literature [3–6] but still remains uncertain. In order to give rise to this plateau, the mean free path, l , of the propagating acoustic excitations has to decrease at least with the fourth power of frequency in the frequency range between some tens of GHz and some THz [1].

The existence in glasses of this strong scattering regime for the acoustic excitations has been predicted in a variety of theoretical models. In the simplest approaches, the material is treated as an elastic medium. The addition of localized impurities gives rise to a sound attenuation proportional to the fourth power of frequency, known as Rayleigh scattering [7,8]. The same law is found in models where the atoms vibrate either on a lattice with random elastic constants [9], or off lattice around a topologically disordered configuration [10]. The same frequency dependence is finally found as well in the soft potential model as a resonant interaction between vibrational soft modes and sound waves [4]. In all of these models, the acoustic wave damping follows this Rayleigh-like law at frequencies below the BP position.

In addition to Rayleigh scattering, many other sound attenuation channels are present in glasses: tunneling in two level systems [11], thermally activated relaxation processes [11], and anharmonicity [12]. From ultrasonic [13] and Brillouin light scattering (BLS) [14] experiments, it is

known that the acoustic attenuation at frequencies $\nu < 50$ GHz is strongly temperature dependent, and thus dominated by the above contributions. On the contrary, the Rayleigh-like attenuation induced by structural disorder is a temperature independent process that becomes relevant only at higher frequencies, since its frequency dependence is much stronger than that of relaxation and/or anharmonic terms. However probing the frequency interval between tens of GHz and a few THz and disentangling the various attenuation mechanisms represents a clear experimental challenge, and the frequency and temperature dependence of the acoustic attenuation in glasses in this range is a matter of active research. Evidences of a Rayleigh-like growth of the sound attenuation in a frequency range just below the BP position have been obtained in only a few systems by means of inelastic x-ray scattering (IXS): permanently densified vitreous silica [15], a lithium borate glass [16], and glycerol [17]. In all of these cases, the sound attenuation is characterized by a crossover frequency, ν_c , below which it follows a ν^4 frequency dependence, which turns into a quadratic law above ν_c . The crossover frequency is found to be close to the BP position.

The most widely studied, prototypical glass is surely vitreous silica. Its acoustic dynamics in the THz frequency regime has been investigated in a number of IXS studies [18–22], and no evidence was found for the crossover frequency ν_c . Controversial results have been reported on the frequency dependence of the sound attenuation at lower frequencies. A Brillouin ultraviolet scattering (BUVS) experiment performed on a bulk sample, showed evidence of the onset of the strong scattering regime, an increase in the sound attenuation compatible with a ν^4 law, at 150 GHz [23]. The observation of ν_c at such low frequency would exclude any connection with the BP, which is found at much higher frequencies of ~ 1 THz [2]. A more recent work reported a contrasting result, showing a much smoother frequency dependence of the sound attenuation up to 300 GHz [24]. In this case, however, the measure-

ments were performed on thin films, leaving some doubts on whether they can be considered valid for the bulk sample as well. In this Letter, we present compelling experimental evidence that the expected crossover is located in the THz frequency range. Recent advancements in the IXS technique, in terms of instrumental resolution, x-ray beam intensity and overall beam line stability [25], finally allow us to unveil a complex phenomenology, hidden by error bars in previous experiments. Our results show that the propagation of the acoustic modes is strongly perturbed around the BP position. In particular, at frequencies lower than that of the BP, the sound attenuation follows a Rayleigh scattering law while the sound velocity is marked by a negative dispersion.

The experiment has been performed at the IXS beam line ID16 of the ESRF in Grenoble, France. A high energy resolution of 1.4 meV is reached at an incident energy of 23.7 keV. The Q resolution is fixed to 0.3 nm^{-1} . In the relevant wave vector range ($Q < 4 \text{ nm}^{-1}$) two spectra are collected simultaneously, using two of the nine available analyzer crystals. The sample is a Suprasil fused-quartz cylinder purchased from Goodfellow with a thickness of 3.5 mm to match the photoelectric absorption length of SiO_2 at the chosen incident energy. The experiment is performed at a temperature $T = 1620 \text{ K}$, i.e., in the supercooled liquid phase, in order to enhance the inelastic signal. More importantly, at this high temperature the BP position is 50% higher in frequency with respect to room temperature. This allows us to measure the Brillouin peaks at frequencies below the BP position, a region inaccessible at lower temperatures. The absence of crystallization has been checked regularly during the experiment by measuring the static structure factor. A selection of spectra is presented in Fig. 1. Each spectrum has been integrated 12 hours to reach the final signal to noise ratio.

The measured intensity is proportional to the dynamic structure factor convoluted with the instrument response function. The dynamic structure factor is modeled as the sum of a delta function to describe the elastic line plus a damped harmonic oscillator (DHO) for the inelastic contribution [22]

$$\frac{S(Q, \omega)}{S(Q)} = f(Q)\delta(\omega) + (1 - f(Q))\frac{1}{\pi} \times \frac{\Omega^2(Q)\Gamma(Q)}{[\omega^2 - \Omega^2(Q)]^2 + \omega^2\Gamma^2(Q)}. \quad (1)$$

The parameters $\Omega(Q)$ and $\Gamma(Q)$ represent the position and width (FWHM) of the inelastic peaks in the measured spectra, $S(Q)$ is the static structure factor, and $f(Q)$ is the nonergodicity parameter. The best fitted line shapes obtained with this model are plotted in Fig. 1. The fit takes into account also the effect of the finite Q resolution of the experiment which induces an additional broadening of the peaks, more relevant at small wave vectors. In the right column of Fig. 1, the inelastic part of the measured dy-

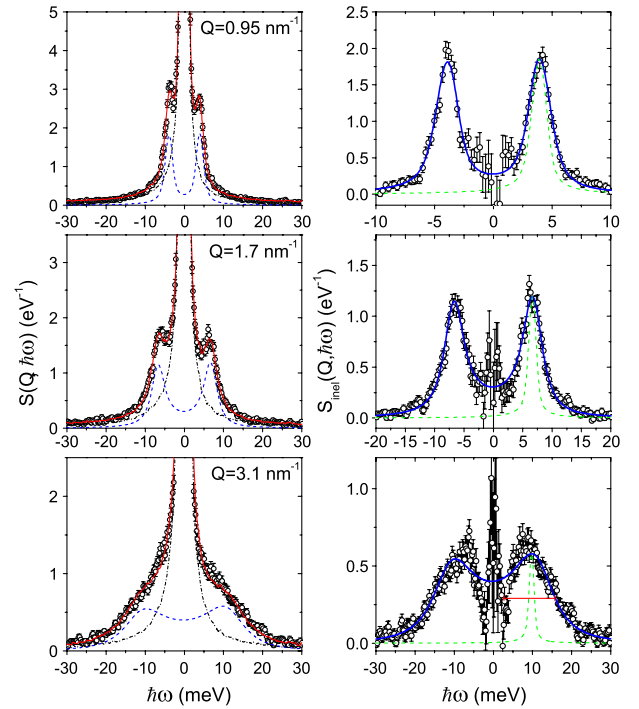


FIG. 1 (color online). Left column: Selection of IXS spectra of $v\text{-SiO}_2$ as a function of ω at the three indicated wave vectors Q . The continuous line (red) is the best fitted function using Eq. (1), convoluted with the resolution function. The elastic (dash-dotted, black) and inelastic (dashed, blue) components are also shown. Right column: inelastic part of the dynamic structure factor. The continuous line (blue) is the best fitted DHO profile, convoluted with the instrument response function (dashed, green). The horizontal line (red), placed at the half maximum of the fit in the lowest panel, is the sum of the unconvoluted DHO model width and of the instrumental width.

amic structure factor is compared to the DHO profile. The broadening of the peak over the instrument resolution width is measurable in the whole explored Q range, and strongly increases with increasing Q . At the highest plotted Q , the DHO fails to properly describe the spectrum, in particular, around $\omega = 0$ [15,16]. Nevertheless the width of the peak is still well described by the DHO model as shown in the lower panel of the figure. The exchanged momentum dependence of the position and width of the inelastic peak derived from the fit analysis is presented in Fig. 2. At first sight, the dispersion relation, $\Omega = \Omega(Q)$, appears to be linear and in agreement with the extrapolation of the macroscopic speed of sound measured by BLS [26]. Looking more closely at the dispersion curve, one finds that it is in fact not perfectly linear. The apparent sound velocity, $v = \Omega(Q)/Q$, plotted as a function of frequency ($\Omega/2\pi$) in the upper panel of Fig. 3, is marked by a negative dispersion at low frequency followed by a positive dispersion at higher frequencies. A speed up of the phase velocity has been already discussed in the literature [21,22]. On the contrary, the mode softening was not

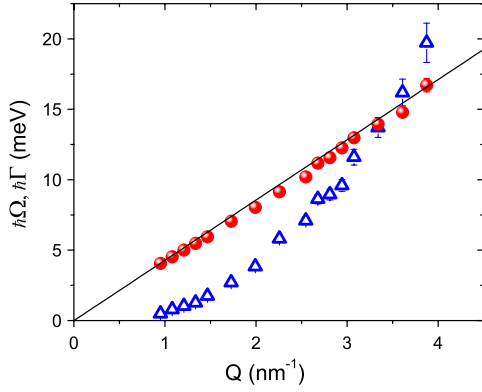


FIG. 2 (color online). Exchanged momentum dependence of the position (circles, red), $\hbar\Omega(Q)$, and of the damping (triangles, blue), $\hbar\Gamma(Q)$, of the acoustic excitations. The line is the linear dispersion at the macroscopic speed of sound [26].

observed before. A similar negative dispersion of the apparent sound velocity has been recently observed also in the glass of glycerol [17].

The mode softening takes place in a frequency range where the sound attenuation shows a frequency dependence compatible with the Rayleigh law, $\Gamma \sim \nu^4$, as shown in the middle panel of Fig. 3. Above a crossover frequency $\nu_c \sim 1.5$ THz, the sound attenuation follows a ν^2 frequency dependence. The lower panel of the figure shows the temperature evolution of the BP as measured by neutron scattering [27,28]. At the temperature of the IXS experiment, the BP frequency coincides with ν_c . The vertical dashed line highlights the fact that these elastic anomalies, negative dispersion and transition between ν^4 to ν^2 in the damping, are directly connected to the excess of modes at the BP. It is also of interest to estimate the Ioffe-Regel crossover frequency, defined by the condition that the acoustic excitation decays in half of the oscillation period, i.e., by the relation $\Gamma = \omega/\pi$ [16]. As shown in the middle panel of Fig. 3, the Ioffe-Regel frequency (the intersection of the data with the dotted line) is very close to the BP frequency.

The complex behavior of both the phase velocity and the damping around the BP position was not detected in previous IXS experiments [18,20]. The new data have error bars 10 times smaller with respect to the previous ones. The points spread in the previous measurements prevented the observation of the fine features reported here. In particular, the strong scattering regime was not visible in previous experiments because of the large error bars affecting the data at frequencies below the BP.

We now compare the new IXS data with analogous measurements performed in other frequency ranges. The sound attenuation is plotted in Fig. 4 as a function of frequency in a log-log plot. In the low frequency range, $\nu < 300$ GHz, the damping at room temperature follows an almost quadratic frequency dependence, which results from the combination of the effects of the anharmonicity of

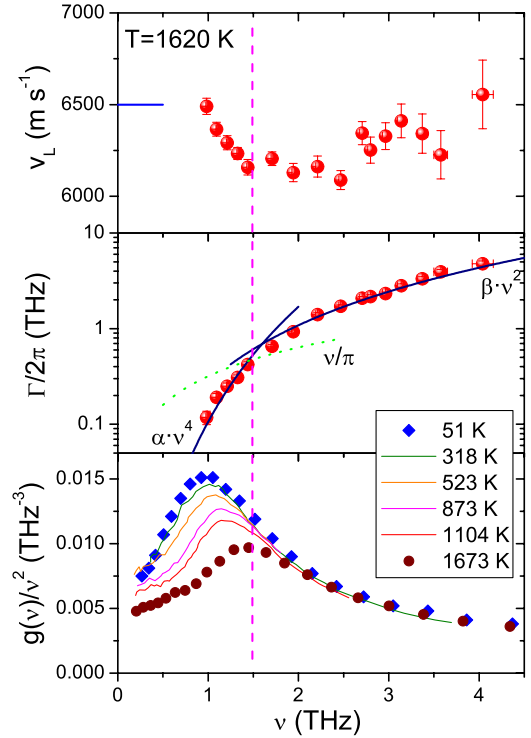


FIG. 3 (color online). The apparent sound velocity (upper panel) and attenuation (middle panel) from the IXS data are plotted as a function of frequency $\nu = \Omega/2\pi$. The lower panel presents the reduced density of states at the indicated temperatures as measured by neutron scattering (Refs. [27,28]). The vertical dashed line (magenta) is placed at the position of the BP at the temperature of the IXS measurement. The line in the upper panel marks the low frequency value for the sound velocity [26]. The continuous lines (navy) in the middle panel are fits to the slopes $\alpha\nu^4$ and $\beta\nu^2$, with $\alpha = (0.106 \pm 0.006)$ THz $^{-3}$ and $\beta = (0.271 \pm 0.007)$ THz $^{-1}$. The dotted line (green) corresponds to the data for ν/π : its intersection with the $\Gamma/(2\pi)$ data defines the Ioffe-Regel limit [16].

the interatomic potential and of thermally activated relaxations [24]. This behavior can be directly compared to the new data at 1620 K, since at GHz frequencies the attenuation above room temperature is almost constant [29]. The ν^2 law extrapolates to the first point of the IXS data. Here the disorder induced term, Rayleigh-like scattering, overcomes the anharmonic or relaxational contributions. The change in slope in the frequency dependence of the sound attenuation observed by means of BUVS [23] is then here clarified not to be related to the onset of the strong scattering regime, which is found at higher frequencies, as shown by the blue line in Fig. 4. A further confirmation of this picture comes from the comparison with the sound attenuation measured by means of the tunneling junction (TJ) method at low temperatures, $T = 1$ K [30]. At 100 GHz there is 1 order of magnitude difference in the attenuation as measured by BUVS at room temperature and by the TJ technique, showing that in the BUVS range

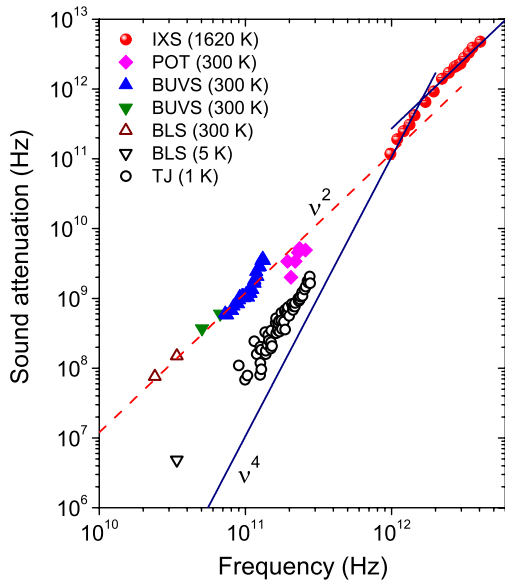


FIG. 4 (color online). Sound attenuation, $\Gamma(\nu)/2\pi$, of ν -SiO₂ as a function of frequency in log-log scale. The points at high frequency (red circles) are from the present work at $T = 1620$ K. Lower frequencies data are from: picosecond optical technique (POT) [24], BUVS [23,31], BLS [14], and a tunneling junction (TJ) technique [30]. The dashed line (red) is a quadratic frequency slope. The blue lines are the two power law fits to the IXS data, $\Gamma \sim \nu^4$ and $\Gamma \sim \nu^2$, presented in the middle panel of Fig. 3.

the sound attenuation is still dominated by anharmonicity or relaxations. The physical origin of the increase in attenuation observed by BUVS should then be considered at the moment unknown. It is also worth noticing that the low temperature data, i.e., the TJ ones at 1 K and the BLS result at 5 K, remain higher than the ν^4 law extrapolated from the IXS data. This discrepancy can be attributed to two mechanisms. The first one is the attenuation at low temperatures due to tunneling in two level systems. The second mechanism is the expected shift of the Rayleigh term with temperature, following the evolution of the BP.

In conclusion, we have reported on a new experimental determination of the elastic properties of the silica glass by means of high resolution IXS. The data give clear evidence of a Rayleigh scattering regime. This observation represents the first direct measurement of the Rayleigh law up to the BP frequency in vitreous silica, confirming the theoretical prediction of the existence in glasses of this peculiar attenuation mechanism. A second new observation is the presence of a softening of the acoustic modes in the frequency range where they experience strong scattering. These anomalies in the wave propagation are intimately connected one to the other, since the apparent sound velocity and the damping parameter are related to the real and

imaginary part of the complex self-energy of the system [22]. A strong increase in the damping is thus reflected in a reduction of the sound velocity. The mode softening observed here indicates that the Debye continuum approximation breaks down at frequencies close to the BP and that the acoustic like modes pile up there, contributing then to the BP excess.

*giacomo.baldi@esrf.fr

- [1] R. C. Zeller and R. O. Pohl, *Phys. Rev. B* **4**, 2029 (1971).
- [2] U. Buchenau *et al.*, *Phys. Rev. Lett.* **53**, 2316 (1984).
- [3] P. Sheng and M. Zhou, *Science* **253**, 539 (1991).
- [4] U. Buchenau *et al.*, *Phys. Rev. B* **46**, 2798 (1992).
- [5] R. Vacher *et al.*, *Phys. Rev. B* **56**, R481 (1997).
- [6] W. Schirmacher, *Europhys. Lett.* **73**, 892 (2006).
- [7] J. W. S. Rayleigh, *The Theory of Sound* (MacMillan, London, 1896).
- [8] P. G. Klemens, *Proc. Phys. Soc. London Sect. A* **68**, 1113 (1955).
- [9] W. Schirmacher *et al.*, *Phys. Rev. Lett.* **81**, 136 (1998).
- [10] T. S. Grigera *et al.*, *Phys. Rev. Lett.* **87**, 085502 (2001).
- [11] J. Jackle *et al.*, *J. Non-Cryst. Solids* **20**, 365 (1976).
- [12] A. Akhiezer, *J. Phys. (USSR)* **1**, 277 (1939).
- [13] R. E. Strakna and H. T. Savage, *J. Appl. Phys.* **35**, 1445 (1964).
- [14] R. Vacher and J. Pelous, *Phys. Rev. B* **14**, 823 (1976); R. Vacher *et al.*, *Phys. Rev. B* **21**, 5850 (1980).
- [15] B. Rufflé *et al.*, *Phys. Rev. Lett.* **90**, 095502 (2003).
- [16] B. Rufflé *et al.*, *Phys. Rev. Lett.* **96**, 045502 (2006).
- [17] G. Monaco and V. M. Giordano, *Proc. Natl. Acad. Sci. U.S.A.* **106**, 3659 (2009).
- [18] P. Benassi *et al.*, *Phys. Rev. Lett.* **77**, 3835 (1996).
- [19] M. Foret *et al.*, *Phys. Rev. Lett.* **77**, 3831 (1996); C. Masciovecchio *et al.*, *Phys. Rev. B* **55**, 8049 (1997); F. Sette *et al.*, *Science* **280**, 1550 (1998); O. Pilla *et al.*, *Phys. Rev. Lett.* **85**, 2136 (2000).
- [20] T. Scopigno, Laurea thesis, L'Aquila University (Italy), 1998; G. Ruocco *et al.*, *Phys. Rev. Lett.* **83**, 5583 (1999); C. Masciovecchio *et al.*, *Philos. Mag. B* **79**, 2013 (1999).
- [21] B. Ruzicka *et al.*, *Phys. Rev. B* **69**, 100201(R) (2004).
- [22] G. Baldi *et al.*, *Phys. Rev. B* **77**, 214309 (2008).
- [23] C. Masciovecchio *et al.*, *Phys. Rev. Lett.* **97**, 035501 (2006).
- [24] A. Devos *et al.*, *Phys. Rev. B* **77**, 100201(R) (2008).
- [25] More details on the beam line layout are available online: <http://www.esrf.fr/UsersAndScience/Experiments/DynExtrCond/ID16/CE/BeamlineLayout>.
- [26] A. Polian *et al.*, *Europhys. Lett.* **57**, 375 (2002).
- [27] A. Wischnewski *et al.*, *Phys. Rev. B* **57**, 2663 (1998).
- [28] A. Fontana *et al.*, *Europhys. Lett.* **47**, 56 (1999).
- [29] J. A. Bucaro and H. D. Dardy, *J. Appl. Phys.* **45**, 5324 (1974).
- [30] W. Dietsche and H. Kinder, *Phys. Rev. Lett.* **43**, 1413 (1979).
- [31] P. Benassi *et al.*, *Phys. Rev. B* **71**, 172201 (2005).